

available at www.sciencedirect.comwww.elsevier.com/locate/brainres

**BRAIN
RESEARCH**

Research Report

Cerebrospinal fluid to brain transport of manganese in a non-human primate revealed by MRI

Nicholas A. Bock^{a,*}, Fernando F. Paiva^a, George C. Nascimento^a,
John D. Newman^b, Afonso C. Silva^a

^aCerebral Microcirculation Unit, Laboratory of Functional and Molecular Imaging, National Institute of Neurological Disorders and Stroke, National Institutes of Health, 10 Center Drive, Building 10, Room BD109, Bethesda, Maryland, 20892-1065, USA

^bDevelopmental Neuroethology Unit, Laboratory of Comparative Ethology, National Institutes of Child Health and Human Development, National Institutes of Health, NIH Animal Center, Poolesville, MD 20837, USA

ARTICLE INFO
Article history:

Accepted 18 December 2007

Available online 4 January 2008

Keywords:

Manganese

Brain

Rat

Marmoset

Magnetic resonance imaging

ABSTRACT

Manganese overexposure in non-human primates and humans causes a neurodegenerative disorder called manganism thought to be related to an accumulation of the metal in the basal ganglia. Here, we assess changes in the concentration of manganese in regions of the brain of a non-human primate (the common marmoset, *Callithrix jacchus*) following four systemic injections of 30 mg/kg MnCl₂ H₂O in the tail vein using T₁-weighted magnetic resonance imaging (MRI) and compare these to changes in the rat following the same exposure route and dose. The doses were spaced 48 h apart and we imaged the animals 48 h after the final dose. We find that marmosets have significantly larger T₁-weighted image enhancements in regions of the brain compared to rats, notably in the basal ganglia and the visual cortex. To confirm this difference across species reflects actual differences in manganese concentrations and not variations in the MRI properties of manganese, we measured the longitudinal relaxivity of manganese (ρ_1) in the in vivo brain and found no significant species' difference. The high manganese uptake in the marmoset basal ganglia and visual cortex can be explained by CSF-brain transport from the large lateral ventricles and we confirm this route of uptake with time-course MRI during a tail-vein infusion of manganese. There is also high uptake in the substructures of the hippocampus that are adjacent to the ventricles. The large manganese accumulation in these structures on overexposure may be common to all primates, including humans.

Published by Elsevier B.V.

1. Introduction

The metal manganese (Mn) is an essential trace element in the brain, found primarily in mitochondrial superoxide dismutase and glutamine synthetase metalloproteins (Takeda, 2003). Following overexposure in humans, however, it is neurotoxic (Crossgrove and Zheng, 2004) and produces manganism — a

motor disorder with similarities to Parkinson's disease (Dobson et al., 2004; Aschner et al., 2005; Antonini et al., 2006; Cersosimo and Koller, 2006). The late-stage symptoms include generalized bradykinesia, widespread rigidity, and occasional resting tremor (Pal et al., 1999) and are thought to be related to an accumulation of manganese in the substructures of the basal ganglia, particularly the globus pallidus. While the exact mechanism of

* Corresponding author. Fax: +1 301 480 2558.

E-mail address: bockn@mail.nih.gov (N.A. Bock).

Table 1 Brain tissue manganese concentration after overexposure

Region	Marmoset		Rat	
	Control	Mn-injected	Control	Mn-injected
Frontal cortex	0.63±0.13	2.92±0.56 ⁺ *	0.52±0.07	1.52±0.30 [*]
Striatum	1.16±0.39	4.45±2.02 ⁺ *	0.58±0.05	2.38±0.32 [*]
Thalamus	1.04±0.41	4.03±1.81 ⁺ *	0.49±0.05	2.12±0.42 [*]
Hippocampus	0.83±0.64	3.08±1.19 ⁺ *	0.58±0.05	1.78±0.29 [*]

Manganese concentration ($\mu\text{g/g}$ wet tissue, mean \pm SD, $n=4$) in excised brain tissue samples before and after four injections of 30 mg/kg $\text{MnCl}_2 \cdot 4\text{H}_2\text{O}$. The asterisk denotes a significant increase over control in the same species ($p < 0.05$). The cross denotes a significant increase in manganese concentration in the marmoset versus the rat ($p < 0.05$).

toxicity is unclear, studies in rodents and non-human primates have shown reduced dopamine (DA) levels in this structure following manganese exposure, suggesting the metal somehow disrupts the DA system (Gwiazda et al., 2007). As well, a study in macaques noted gliosis in the globus pallidus and the substantia nigra reticularis (Olanow et al., 1996). Manganese poisoning can also produce symptoms not specifically related to the basal ganglia including cognitive impairments (Klos et al., 2006) and memory loss (Bowler et al., 2006), suggesting it has toxic effects in other brain regions.

Exposure to manganese in humans occurs through inhalation of aerosols or dusts that contain high levels of the metal

(Antonini et al., 2006; Cersosimo and Koller, 2006) as well as through diet (Erikson et al., 2007). Blood levels of manganese are also increased in patients with reduced liver function (Park et al., 2003), since the major mode of excretion is through bile. Studies in animals addressing the uptake of manganese specifically into brain tissue have identified three routes: 1 from the bloodstream through the cerebral spinal fluid (CSF) via the choroid plexus (Murphy et al., 1991; Aoki et al., 2004), 2 from the nasal space through the olfactory nerve via the olfactory epithelium (Tjalve et al., 1996, 1995; Pautler and Koretsky, 2002), and 3 from the bloodstream across the blood–brain-barrier (BBB) at the cerebral capillaries (Crossgrove et al., 2003; Rabin et al., 1993). It is not clear whether one route dominates uptake in cases of manganese poisoning in non-human primates and humans. Once inside the brain, manganese can be transported along axons (Sloot and Gramsbergen, 1994) and across synapses (Pautler et al., 2003); thus, its overall distribution can change with time. This means that regions with initial poor access to manganese may be supplied over time by axonal transport from other regions with strong initial uptake. The clearance of manganese from brain tissue is very slow, with a half-life of 51–74 days in different regions (Takeda et al., 1995).

An interesting physical property of manganese is that it is highly paramagnetic and can be detected in vivo in the brain with magnetic resonance imaging (MRI) because it shortens the longitudinal relaxation time (T_1) of tissue. Studies addressing manganese overexposure in humans and non-human primates using MRI have described T_1 -weighted image enhancements in

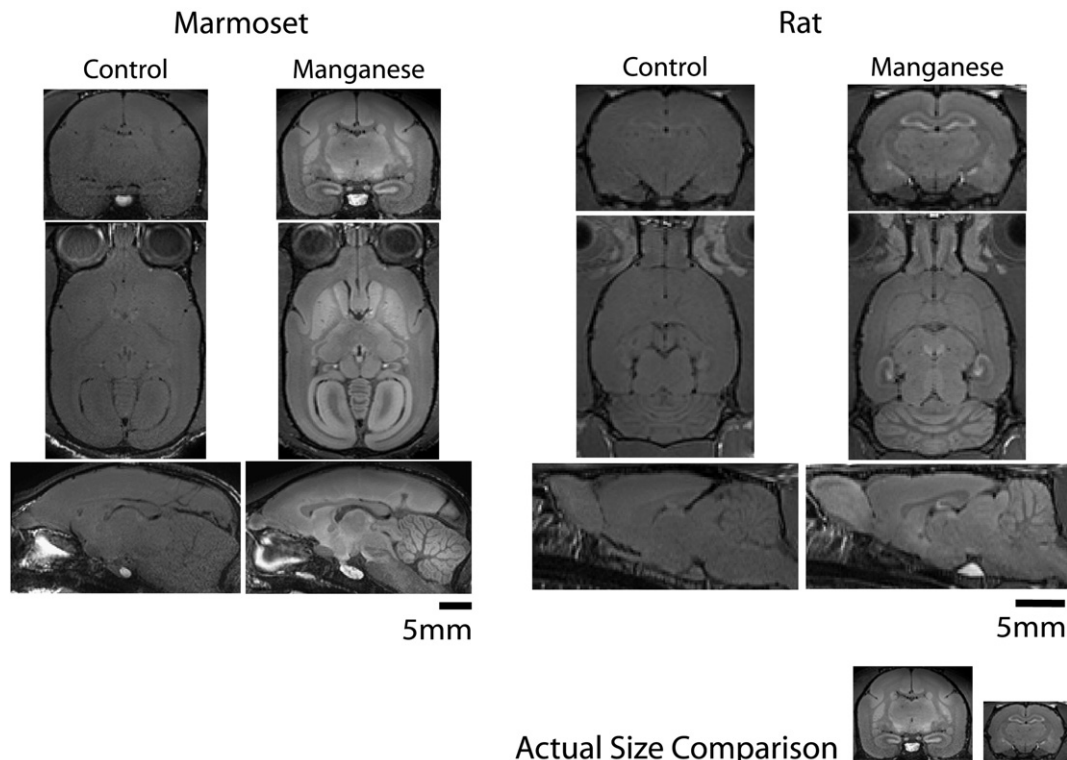


Fig. 1 – T_1 enhancement in the marmoset and rat brain with manganese overexposure. Coronal (Top), horizontal (Middle) and sagittal (Bottom) slices are shown from a 3D T_1 -weighted image of a control marmoset and rat (First and Third Columns), and a marmoset and rat following four 30 mg/kg injections of $\text{MnCl}_2 \cdot 4\text{H}_2\text{O}$ (Second and Fourth Columns). The manganese images were made 48 h after the fourth injection. The marmoset shows stronger T_1 -weighted image enhancement following the manganese injections than the rat.

the basal ganglia, most notably in the globus pallidus and substantia nigra (Uchino et al., 2007; Pal et al., 1999; Jiang et al., 2007; Krieger et al., 1995; Dorman et al., 2006b; Shinotoh et al., 1995; Guilarte et al., 2006). In fact, T_1 -weighted hyperintensity in the basal ganglia is used as a biomarker for manganese poisoning in humans (Jiang et al., 2007). MRI is an important assay for manganese, since there is no histological stain for it and its accumulation must otherwise be measured in brain tissue samples with techniques such as mass spectrometry or with a ^{54}Mn radioactive tracer. This limits detection to regions that can be unambiguously identified and dissected for analysis and precludes longitudinal studies in the same subject.

Recently, detailed MRI studies of the *in vivo* distribution of manganese across the whole rodent brain have been performed, cataloguing the regions where it accumulates (Natt et al., 2002; Aoki et al., 2004). As well, MRI studies have shown that a CSF-brain route is the primary mechanism of uptake in the rodent brain and the majority of strongly enhancing structures seen on T_1 -weighted images are adjacent to ventricles (Aoki et al., 2004; Lee et al., 2005). Unlike humans or non-human primates, however, rodents do not develop serious neurobehavioural clinical signs following manganese overexposure. Whether this is due to differences in the distribution of manganese in the central nervous system (CNS) between species or intrinsic differences in tissue sensitivity is unknown.

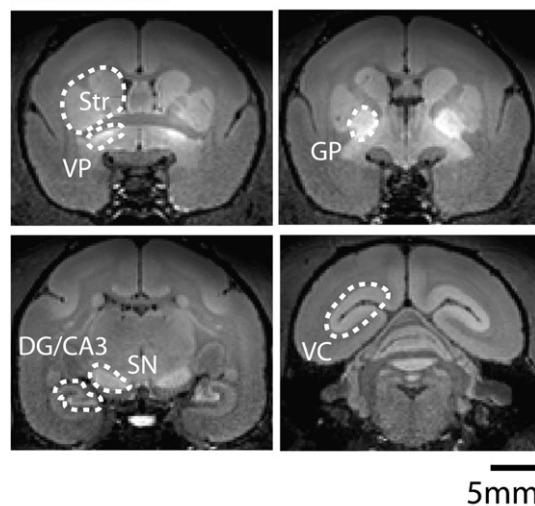
In this paper, we use MRI and inductively-coupled plasma mass spectrometry (ICPMS) to assay increases in manganese concentration in the brain of a small non-human primate (the common marmoset, *Callithrix jacchus*) following a short series of fractionated systemic injections of Mn^{2+} into the tail vein. We use fractionated injections to build a detectable dose of manganese in the brain while limiting the toxic effect in other organs (Bock et al., *in press*). We also perform the same protocol in similarly-sized rats to directly compare the accumulation in non-human primates to the accumulation in rodents, which are the more common animals for toxicology studies. Our results show that marmosets accumulate more manganese than rats do at a comparable exposure dose in the brain, notably in the regions of the basal ganglia and the visual cortex. We hypothesize this is because the CSF-brain uptake route also dominates uptake in the non-human primate brain, and these structures are proximal to the large CSF space in the non-human primate lateral ventricles.

2. Results

Table 1 shows the concentration of manganese measured by ICPMS in tissue samples of brain regions in marmosets and rats without and with four systemic injections of 30 mg/kg $\text{MnCl}_2 \cdot \text{H}_2\text{O}$ in the tail vein. Following injections, the increases in the concentration of manganese in structures of the marmoset brain were statistically greater than those in the same structures in the rat brain ($p < 0.05$)—in all structures, the difference is almost two-fold, although both species are about the same weight and the injected dose amount is normalized to the body weight.

For a more spatially detailed analysis of brain manganese distribution, we used *in vivo* high resolution 3D T_1 -weighted MRI. Figs. 1 and 2 summarize the T_1 -weighted MRI enhancement in representative slices from 3D images in the two species before

Marmoset



Rat

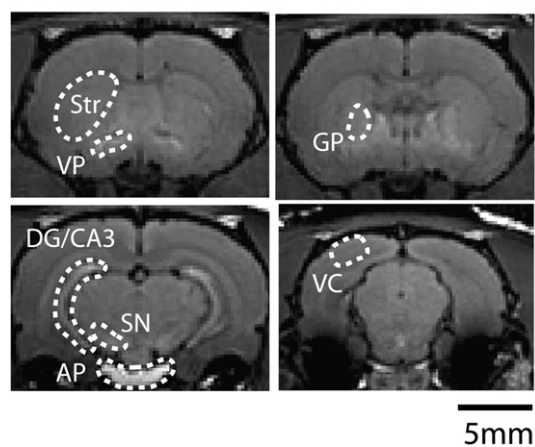


Fig. 2 – Increased T_1 enhancement in the structures of the marmoset basal ganglia and visual cortex. Coronal slices are shown from a 3D T_1 -weighted image in a representative marmoset and rat. (Str = striatum, VP = ventral pallidum, GP = globus pallidus, DG/CA3 = dentate gyrus and CA3 regions of the hippocampus, SN = substantia nigra, AP = anterior pituitary, VC = visual cortex). Note that neither the internal and external segments of the globus pallidus, nor the compact and reticular parts of the substantia nigra can be separated on the MRI.

and after manganese exposure. Immediately, it is evident that not only is there greater signal enhancement in the marmoset brain, but the pattern of enhancement is significantly different from the rat. This can readily be seen in the increased enhancement in the basal ganglia and visual cortex in the marmoset (Fig. 2). To catalogue major enhancing structures in both species, we plot the normalized signal intensities in different regions (Fig. 3). It should be noted that MRI is less sensitive to changes in manganese concentration than mass spectrometry (see section on Interpretation of T_1 -weighted images in Experimental procedures). However, we did detect statistically significant large increases in enhancement in several structures in both species, as well as statistically significant differences in the pattern of enhancement between the species. There were

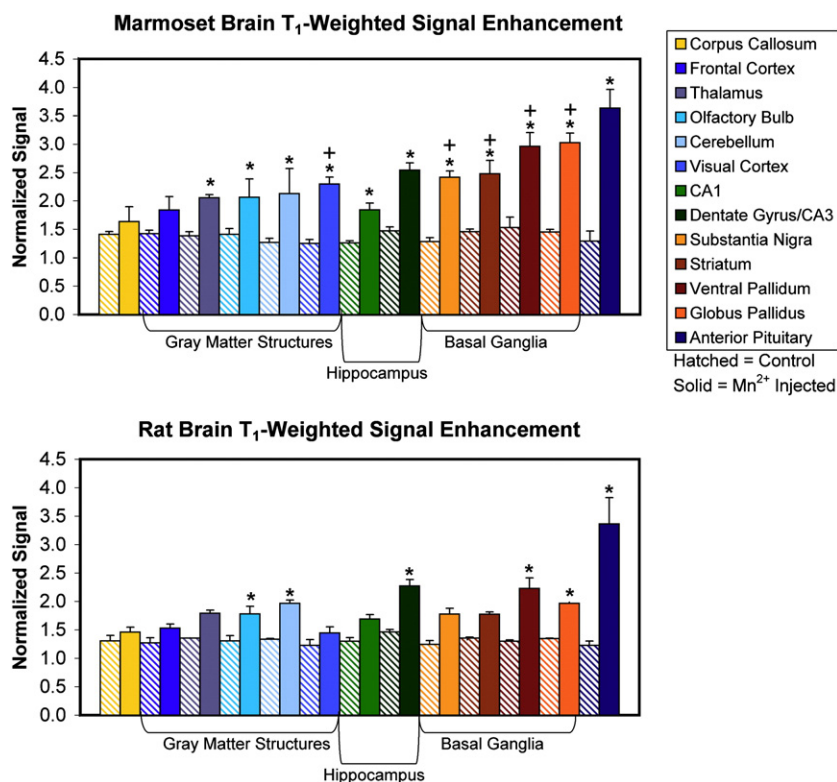


Fig. 3 – T₁-weighted signal enhancements in the marmoset and rat brain. The asterisk denotes regions that were significantly enhanced in the marmosets or the rats following manganese overexposure ($p < 0.05$). The crosses denote regions that were significantly more enhanced in the marmoset than in the rat ($p < 0.05$). Error bars are standard deviations, $n = 4$ for each data point.

small increases in enhancement throughout the brain that did not make statistical significance. This does not mean, however, that these structures did not accumulate manganese — to accurately quantify this requires a more sensitive ex vivo technique like ICPMS. At one end of the plot is the corpus callosum, a white matter structure with no statistically significant enhancement

in either species ($p = 1.00$) while at the other end the anterior pituitary gland, a structure lacking a BBB with the largest increase in enhancement in the brain ($p < 0.05$). Neither species has statistically significant enhancement in the frontal cortex ($p = 1.00$). The marmoset has statistically significant enhancement in the thalamus ($p < 0.05$) while the rat does not ($p = 0.14$).

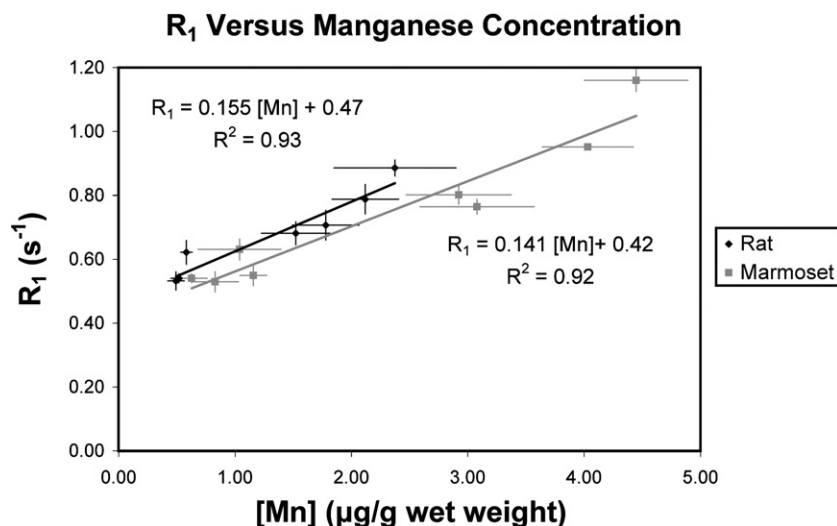


Fig. 4 – In vivo longitudinal relaxivity, χ_1 , of manganese in the marmoset and rat brain. The data is linearly fit to Eq. (2). There is no statistical significance between χ_1 in the marmoset and rat ($p < 0.05$). Error bars are standard deviations, $n = 4$ for each data point. Note that $R_1(0)$ does not have a biological interpretation because there are always trace amounts of manganese present in the brain.

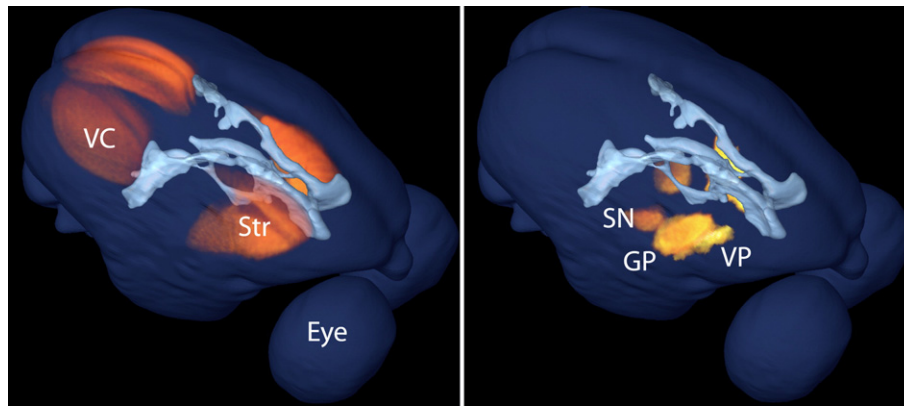


Fig. 5 – Relationship of several strongly enhancing regions in the marmoset to the ventricles. The figure shows a 3D volume rendering of a T_1 -weighted image of a representative marmoset following four injections of 30 mg/kg $MnCl_2 \cdot 4H_2O$ with the CSF in the ventricles shown in light blue. (VC = visual cortex, Str = striatum, SN = substantia nigra, GP = globus pallidus, VP = ventral pallidum).

Both species have statistically significant enhancement in the gray matter of the cerebellum ($p < 0.05$) and in the olfactory bulb ($p < 0.05$). The marmoset has statistically significant enhancement in the visual cortex ($p < 0.05$), a gray matter structure that does not enhance significantly in the rat ($p = 1.00$). The marmoset has statistically significant enhancement in the CA1 region of the hippocampus ($p < 0.05$), although the rat does not ($p = 0.69$). The dentate gyrus and the CA3 region of the hippocampus are significantly enhanced in both species ($p < 0.05$). Finally, in the marmoset, all of the structures of the basal ganglia have statistically significant enhancement ($p < 0.05$), with the globus pallidus showing the highest enhancement. In the rat, the globus pallidus and the ventral pallidum have statistically significant enhancement ($p < 0.05$) but the striatum ($p = 0.26$) and the substantia nigra ($p = 1.00$) do not.

To confirm that the higher T_1 signal enhancement in the marmoset is caused by a larger increase in manganese concentration and not by a difference in the MR properties of manganese, the longitudinal relaxivity, χ_1 , for manganese in the brain must be the same for both species (see section on Interpretation of T_1 -weighted images). In Fig. 4, we determine χ_1 for both species by fitting the data from our T_1 and ICPMS measurements to Eq. (2) (under Interpretation of T_1 -weighted images section). For marmosets $\chi_1 = 0.141 \text{ s}^{-1} \mu\text{g}^{-1} \text{ g}$ and for rats $\chi_1 = 0.155 \text{ s}^{-1} \mu\text{g}^{-1} \text{ g}$. The linear fit to the data is good, suggesting that χ_1 is continuous over the regions we analyzed in both species. There is no significant difference in χ_1 between the two species ($p = 0.54$); thus, our assumption that signal changes in T_1 -weighted images following manganese injections equivalently reflect changes in manganese tissue concentration in the two species is valid. For reference, χ_1 for Mn^{2+} ions in aqueous solution is roughly $0.127 \text{ s}^{-1} \mu\text{g}^{-1} \text{ g}$ ($7 \text{ s}^{-1} \text{ mM}^{-1} \text{ kg}$) (this value is independent of magnetic field strength (Kang and Gore, 1984; Chuang and Koretsky, 2006)).

It is interesting to note the structures that have a significantly greater increase in enhancement in the marmoset versus the rat: the visual cortex, the striatum, the globus pallidus, the ventral pallidum, and the substantia nigra. Fig. 5 shows the location of these structures in the marmoset brain. Two of these structures are proximal to a large volume of CSF in the marmoset but not the rat (Fig. 6). In the marmoset, the visual

cortex is adjacent to the posterior horn of the lateral ventricle. In the rat, the posterior horn does not extend to this structure. As well, the caudate of the striatum in the marmoset forms the lateral wall of the anterior horn and body of the lateral ventricle. While the same is true in the rat, the CSF space is much smaller than in the marmoset (Fig. 6). These two species differences suggest that the CSF-brain route of uptake is important in the marmoset and that the stronger manganese uptake in the marmoset brain is because of the geometry of the lateral ventricles. To confirm this route of uptake, we imaged brain uptake directly

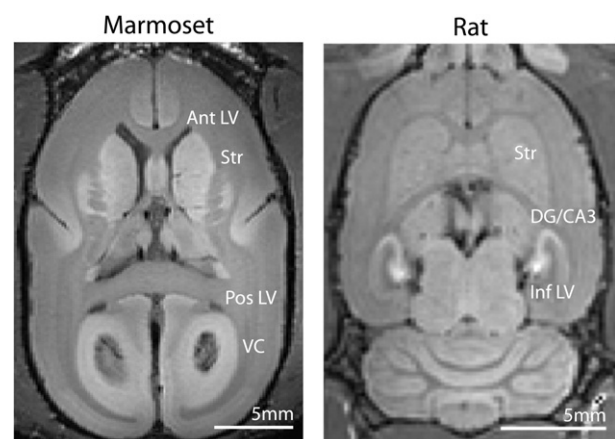


Fig. 6 – Comparison of ventricle geometry and T_1 enhancement in a marmoset and a rat. The in-plane resolution of the images is $223 \mu\text{m}$ (marmoset) and $167 \mu\text{m}$ (rat). The anterior and posterior horns of the marmoset lateral ventricles (which appear dark in the image) are much larger in the marmoset and are proximal to the striatum and the visual cortex which both have strong T_1 enhancement. The inferior horn of the lateral ventricle in the rat is visible in this plane, as is the strong enhancement in the proximal structures of the dentate gyrus and CA3 region of the hippocampus. (Ant LV = anterior horn of lateral ventricle, Str = striatum, Pos LV = posterior horn of lateral ventricle, DG/CA3 = dentate gyrus and CA3 region of the hippocampus). Inf LV = inferior horn of lateral ventricle.

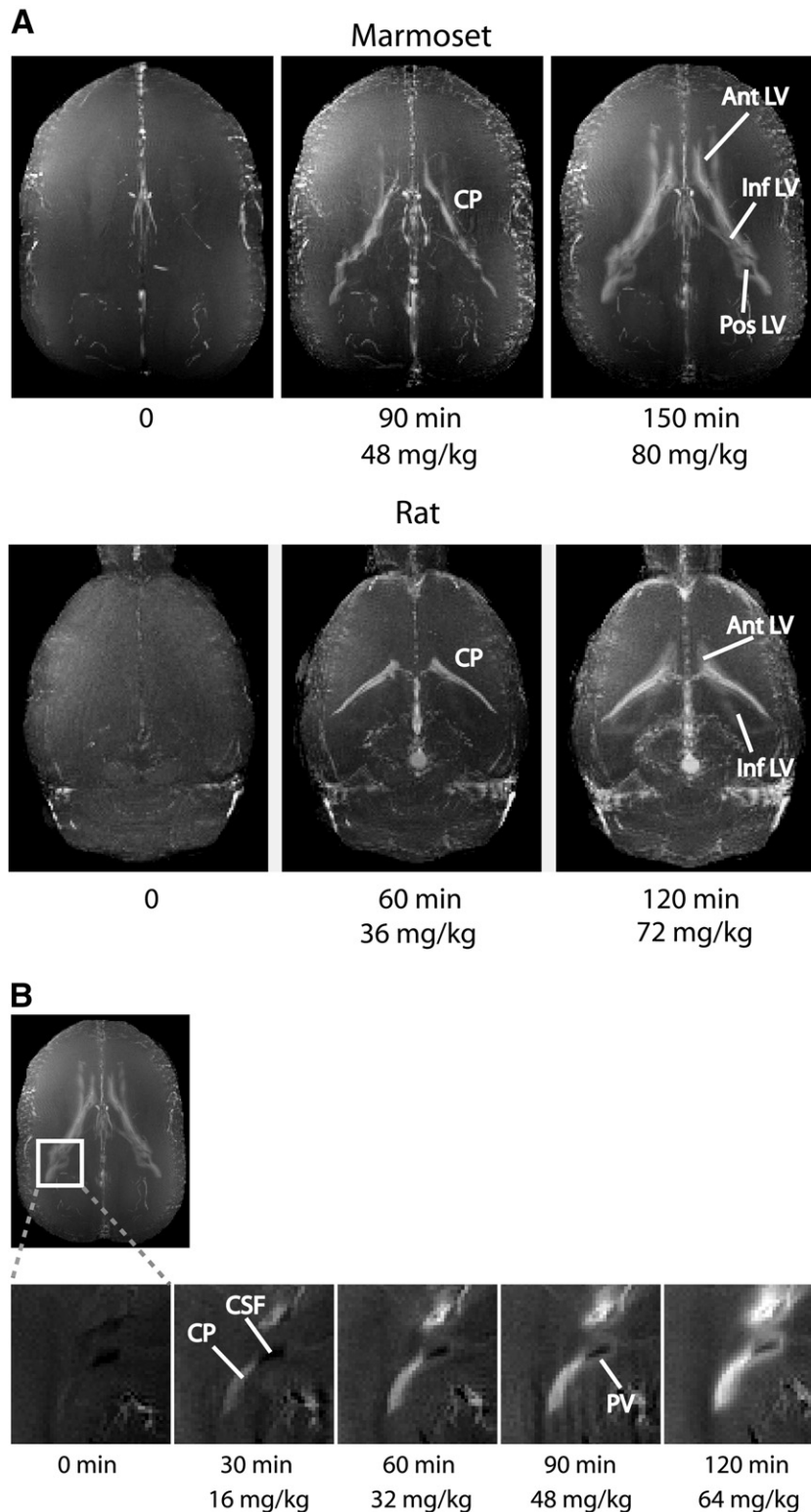


Fig. 7 – a. Periventricular uptake of manganese during an infusion in a marmoset and a rat. The T_1 -weighted images show projections through horizontal slices spanning the lateral ventricles in each species. A 40 mM solution of $MnCl_2 \cdot 4H_2O$ was infused at 1.25 ml/h and the time at the start of each image and the cumulative dry drug/body weight at that time are shown beneath the images. Arteries show bright in this type of image without manganese at 0 min. After 90 min (marmoset) or 60 min (rat) the choroid plexus (CP) shows strong enhancement. As well, enhancement can be seen in the veins and subarachnoid space surrounding the brain. After 150 min (marmoset) or 120 min (rat), strong enhancement can be seen in the parenchyma surrounding the ventricles. There is no visible enhancement in the CSF and there is no visible enhancement from the vasculature or subarachnoid space. **b.** Enlarged region of marmoset brain during a manganese infusion showing periventricular (PV) uptake. The time at the start of each image and the cumulative dose of manganese given by that time are both shown. (CSF = cerebral spinal fluid).

in a marmoset and a rat during a continuous systemic infusion of manganese (Figs. 7a and b). Initially, we detected enhancement in the choroid plexus, blood vessels and the sagittal sinus in both species. As the infusion continued, we observed enhancement in the parenchyma surrounding the ventricles. This periventricular enhancement suggests uptake from the choroid plexus, through the CSF, to the parenchyma. We did not see enhancement in the CSF itself, suggesting the manganese concentration in this pool was too low to affect T_1 . This indicates a fast transfer of manganese from the CSF in the ventricles to the parenchyma. Over the course of the infusion, we did not detect enhancement in parenchyma that was not proximal to the ventricles, suggesting there was little uptake from the blood vessels or the subarachnoid space.

3. Discussion

Our findings show that, as in rodents, a major route of manganese uptake in the non-human primate brain following a systemic exposure is from the bloodstream, across the epithelium of the choroid plexus, into the CSF in the ventricles, and across the ependyma into the parenchyma. Once in the interstitial space of the parenchyma, Mn^{2+} can diffuse and enter excitable cells via voltage-gated Ca^{2+} channels (Lin and Kortschy, 1997; Narita et al., 1990), since the two ions are biological analogues. There are also alternate uptake mechanisms from the interstitial space into neurons and other cells. For example, in the normal brain, 80% of manganese is contained in astrocytes as glutamine synthetase (Wedler and Denman, 1984). However, the specific cellular fate of manganese following overexposure is still unknown.

The CSF-brain uptake theory explains why the majority of structures with high uptake in the marmoset and rat are adjacent to ventricles. For example, the gray matter in the cerebellum in both species is in contact with the fourth ventricle. As well, the dentate gyrus and CA3 region of the hippocampus in both species form the medial wall and floor of the inferior horn of the lateral ventricles. And as we have shown in the marmoset, the visual cortex and the caudate nucleus in the striatum are in contact with the large pool of CSF in the lateral ventricles. Outside of the ventricles in the subarachnoid space, transport may be limited by the presence of pia matter between the CSF and the parenchyma, which would explain why no regions of the cortex in our study other than the visual in the marmoset showed statistically significant image enhancement.

A question remains, however, of the strong uptake in the structures of the basal ganglia in the marmoset that are not in direct contact with ventricles (Fig. 5), especially in the globus pallidus which is thought to figure prominently in manganism. But there is solid evidence that manganese accumulation in these structures is caused by redistribution from the striatum. Two studies in the macaque (Murayama et al., 2006; Saleem et al., 2002) using intrastriatal and intracortical injections of $MnCl_2$ with follow-up MRI have clearly shown efficient anterograde transport of Mn^{2+} from the striatum to the globus pallidus and the substantia nigra, and from the ventral striatum to the ventral pallidum. This would account for the accumulation of manganese in the structures of the basal ganglia in the marmoset following uptake in the striatum from the lateral ventricles. The

weaker accumulation in the basal ganglia of the rat is consistent with a reduced supply of manganese to the striatum because of the small lateral ventricles.

It has previously been suggested that the neurotoxicity of inhaled manganese may be related to uptake in the brain via an olfactory pathway. This nose-to-brain pathway is of interest because occupational manganese toxicity is most frequently linked to inhalation in humans. In this model, manganese is taken up by primary olfactory neurons, and is redistributed to the rest of the brain via secondary, then tertiary neurons in the olfactory pathway (Henriksson et al., 1999). Studies in rhesus monkeys (Dorman et al., 2006a) and rats (Tapin et al., 2006) have shown increased manganese concentrations in the olfactory bulb following inhalation exposure to manganese sulfate. As well, the same studies reported elevated concentrations in the globus pallidus. However, nose-to-brain transport would require a strong direct transport pathway between the olfactory cortex and the globus pallidus to explain the strong uptake in this structure, which has not been demonstrated. Inhalation, however, also leads to a systemic bloodstream exposure because of uptake at the lungs and in the nasal space (Dorman et al., 2006a); thus CSF-brain transport may explain basal ganglia uptake following exposure to airborne manganese, since there are strong transport connections from the striatum to the globus pallidus and the substantia nigra, and the striatum is well supplied with manganese from the CSF in non-human primates.

Another possible explanation for uptake in a region is by a direct route across the BBB of the cerebral capillaries via a manganese transporter. While a unique transporter for manganese has not been shown, it is transported by nonspecific metal transporters including transferrin and divalent metal transporter 1 (DMT1) (Aschner et al., 2007). In fact, DMT1 has been shown to be required for manganese transport across the rat olfactory epithelium (Thompson et al., 2007). We did not see any evidence of direct uptake from the bloodstream into structures not adjacent to the ventricles during our infusion study (Fig. 7). Specifically, there was no immediate enhancement in the marmoset globus pallidus, the region with the strongest eventual enhancement 48 h after injections. It may be, however, that there is a slow uptake of manganese across the BBB that we did not detect during our acute infusion.

Indeed, our study does not rule out the possibility of brain uptake from the olfactory nerve via the olfactory epithelium, or across the BBB at the cerebral capillaries, and both mechanisms may still figure in brain uptake following overexposure. Previous studies have shown that at normal plasma concentrations, transport of manganese across cerebral capillaries dominates, whereas at high plasma concentrations, transport across the choroid plexus is more prevalent (Murphy et al., 1991; Rabin et al., 1993). This indicates that transport depends on the predominant form of manganese in the plasma. We used a high-dose, intravenous bolus of manganese which may have overwhelmed homeostatic mechanisms in the plasma leading to a high fraction of manganese in the free ionic form and an uptake in the brain different from that of chronic, low-dose exposures. Our findings do indicate however, that CSF-brain uptake followed by redistribution through axonal transport is the major route of accumulation for high-dose systemic exposures to manganese. Also, the strong uptake in the structures of the marmoset basal ganglia we observed in our study is

typical of findings in human poisoning cases and low-dose chronic inhalation studies in non-human primates.

It is interesting to translate our findings in marmosets to humans. We confirm the globus pallidus as having the strongest T_1 -enhancement, suggesting this structure accumulates the most manganese on overexposure. There is strong enhancement as well throughout the other structures of the basal ganglia. There is also strong enhancement in the marmoset in the dentate gyrus and CA3 subregions of the hippocampus and in the visual cortex, which are new findings in the non-human primate brain. Since not all of the neurological symptoms of manganism in humans are explained by basal ganglia damage, it is possible that these structures are important in the disease. And if our hypothesis concerning CSF-brain transport of manganese is correct, there may also be uptake in the human frontal cortex, since the lateral ventricles come in close proximity to it. Care must be taken, however, in interpreting the findings in terms of manganism. For instance, the relationship between the manganese concentration and tissue damage is still largely unknown. If a structure is resistant to damage, the fact that it accumulates large amounts of manganese is irrelevant in explaining manganism.

Interestingly, the marmosets had a significantly higher accumulation of manganese than rats in most brain structures studied (see Table 1 and Fig. 3) even though the injected dose was normalized to body weight. Reasons for this difference are not clear. It may be that marmosets have a higher uptake of manganese from the bloodstream into the brain, or that the hepatobiliary clearance of manganese from the bloodstream is slower so that more injected manganese is ultimately available for uptake. The liver is the major organ for manganese excretion (Klaassen, 1974); thus, there is a possibility that a dysfunction of the hepatobiliary system in the marmosets in this study leads to a poor clearance of manganese from the blood and an increased accumulation of the metal in the CNS versus the rats. In fact, although assessing the general toxicity of manganese was not an aim of this study, gross pathology performed post-mortem in the manganese-injected group of marmosets revealed that two of four animals had significant liver damage — the pathological findings were hemosiderosis, congestion, and hepatic necrosis. This suggests marmosets are more susceptible to liver damage than rodents. A previous study in rats have shown that they will tolerate daily injections of 30 mg/kg $MnCl_2 \cdot 4H_2O$ for up to 6 weeks (Zhang et al., 2003) without serious liver complications, while our data suggests that four injections of 30 mg/kg can cause liver damage in a marmoset. Future studies in which the bloodstream concentration of manganese is assessed over time in both species are necessary to determine whether the larger accumulation in the marmoset brain is due to a longer lifetime of manganese in the blood because of poor hepatobiliary clearance or whether uptake into the parenchyma is higher in this species.

In conclusion, our findings show a strong accumulation of manganese in regions adjacent to ventricles in the marmoset brain and suggest that non-human primates are more susceptible to manganese neurotoxicity than rodents because of the large CSF space of the lateral ventricles. In particular, the position of the caudate of the striatum as the medial wall of the anterior horn and body of the lateral ventricles provides good access to the basal ganglia for manganese uptake from the CSF.

This also identifies the choroid plexus as an important location to study the mechanism of manganese transport across the BBB.

4. Experimental procedures

4.1. Animals

All animal experiments were approved by the NINDS/NIDCD/NICHD Animal Care and Use Committees. Experiments were carried out in male and female common marmosets aged 6.5 ± 2.1 years (mean \pm standard deviation, $n=9$) and weighing 362 ± 83 g, and in adult male Sprague–Dawley rats aged 10 weeks and weighing 366 ± 26 g ($n=9$) (Harlan, Indianapolis, IN, USA). Marmosets were housed two to a cage with a twelve-hour light/dark cycle on an ad libitum diet of Purina 5040 biscuits, Zupreem canned marmoset food, unfiltered water, P.R.A.N.G. rehydrator, and fruit and vegetable treats. Rats were also housed two to a cage with a twelve-hour light/dark cycle on an ad libitum diet of Quality Lab Products rat chow and unfiltered water. Cage enrichment was provided for both the marmosets and rats. Four marmosets were used as control animals, four marmosets were given four fractionated injections of manganese over time then imaged with MRI, and one marmoset was given a large single dose of manganese during an MRI imaging session. The same number of rats was used in each experiment as well.

4.2. Experimental design

Initial experiments were performed in a control group of four marmosets and four rats. Two types of MRI were performed in each animal — low resolution 2D multi-slice T_1 -mapping and high resolution, 3D, whole brain T_1 -weighted imaging. Following imaging, the animals were euthanized, the brain tissue was removed, and the manganese content was measured using inductively-coupled plasma mass spectrometry (ICPMS). To assess manganese uptake, a group of four marmosets and a group of four rats were injected with a series of four injections of 30 mg/kg $MnCl_2 \cdot 4H_2O$ in the tail vein spaced 48 h apart and imaged as per the control animals 48 h following the final injection. These animals were euthanized immediately following imaging and brain manganese content was assessed. In a final experiment, one marmoset and one rat were imaged during a tail-vein infusion of manganese in the MRI to observe the acute accumulation of manganese in the brain, specifically around the ventricles.

4.3. Fractionated manganese injections

A 40 mM solution of $MnCl_2 \cdot 4H_2O$ (Sigma Aldrich, St. Louis, MO, USA) was prepared in 200 mM bicine buffer, since Mn^{2+} in solution acts a weak acid. The pH of the solution was corrected to 7.4 using 1 M NaOH. The measured osmolarity was 280 mOsm. Anaesthesia was induced for manganese injections in both species with 5% isoflurane in a 2:2:1 mixture of medical air, nitrogen, and oxygen delivered via a facemask. Anaesthesia was continued with 2% isoflurane in a 2:2:1 mixture of medical air, nitrogen, and oxygen. The isoflurane was varied around 2% to maintain anaesthesia which was monitored by end tidal CO_2 , heart rate, and SPO_2 measurements using a capnograph and

pulse oximeter (Surgivet, Waukesha, WI, USA). The rectal temperature was measured and the animal's body temperature was maintained at 38.5 °C (marmoset) or 37.0 °C (rat) with a water heating pad. A tail-vein catheter was placed in the anaesthetized animal and the MnCl₂ solution was slowly infused at 1.25 ml/h to reduce stress to the heart. A dose of 30 mg/kg MnCl₂ 4H₂O (dry drug weight/body weight) was given to each animal: this represented an average injected volume of solution of about 1.3 ml (marmosets) and 1.4 ml (rats). Animals were returned to their cages after dosing with free access to food and water. After 48 h, the animals received another injection. This was repeated for four doses.

4.4. MRI

Anaesthesia was induced in marmosets with an intramuscular injection of 10 mg/kg ketamine, and in rats with 5% isoflurane. During imaging, the animals were placed on an MRI-compatible cradle and anaesthetized through a nose cone with 2% isoflurane in a 2:2:1 mixture of medical air, nitrogen, and oxygen. Again, the isoflurane was varied around 2% to maintain anaesthesia which was monitored by end tidal CO₂, heart rate, and SPO₂. The rectal temperature was measured and the animal's body temperature was maintained at 38.5 °C with a water heating pad augmented with blown hot air (marmoset) or at 37 °C with a resistive heating pad (rat). MRI was performed on a 7T MRI scanner (Bruker Biospin, Ettlingen, Germany) equipped with a 15 cm gradient set of 450 mT/m strength (Resonance Research Inc., Billerica, MA, USA). A custom-built 16-rung high pass birdcage radiofrequency coil with a 12 cm inner diameter was used for transmission, and a four-element phased-array receiver coil (Bruker Biospin, Ettlingen, Germany) for reception.

Low resolution T₁ mapping was performed using a 2D inversion-recovery EPI sequence (TE=38 ms, TR=9400 ms, FOV=38.4 mm×38.4 mm (marmoset) or 25.6×25.6 mm (rat), Matrix=96×96, Slice thickness=1 mm (marmoset) or 0.75 mm (rat), Slice orientation = coronal, Number of slices=5, Number of inversion times=45, Inversion time increment=200 ms, Number of averages=2), producing an in-plane resolution of 400 μm (marmoset) or 267 μm (rat). The sequence was repeated multiple times to span structures of interest in the brain. The data were fit to a three parameter, single-exponential T₁ recovery function in Matlab (MathWorks, Natick, MI, USA) to produce T₁ maps.

High resolution 3D T₁-weighted imaging was performed with a 3D fast spin-echo with two echoes (TE=11 ms, TR=150 ms, FOV=42.8×42.8×42.8 mm (marmoset) or 42.8×32.0×32.0 mm (rat), Matrix=192×192×192 (marmoset) or 256×192×192, Number of averages=2), producing an isotropic resolution of 223 μm (marmoset) or 167 μm (rat) over the whole brain. B₁ inhomogeneities were corrected using a reference radiofrequency coil method (Wang et al., 2005).

4.5. Brain manganese content

Animals were euthanized under 5% isoflurane with a lethal injection of sodium pentobarbital. The brain was excised and snap frozen in 2-methyl butane (Sigma Aldrich, St. Louis, MO, USA) cooled to just above freezing in liquid nitrogen to prevent diffusion of manganese between brain regions or

from the brain entirely. The brain was partially thawed and then sectioned in 2 mm coronal slices in a brain matrix. Four regions (the frontal cortex, the striatum, the thalamus, and the hippocampus) were identified with the aid of an atlas (Paxinos and Watson, 1998; Stephan et al., 1980) and tissue samples were dissected. Manganese content was analyzed using ICPMS (West Coast Analytical Service, Santa Fe Springs, CA, USA).

4.6. Infusion of manganese in MRI

To study the acute uptake of manganese, we imaged one marmoset and one rat during an infusion of manganese in the MRI. These experiments used a higher dose of manganese than the fractionated injections to help visualize early enhancement around the ventricles. Animals were anaesthetized with 2% isoflurane and monitored as in the other MRI experiment. A tail-vein catheter was placed and the animal was loaded in the MRI. Time-course imaging was performed with a 2D FLASH sequence (TE=4.8 ms, TR=200 ms, Flip angle=60, FOV=44.8×44.8 mm (marmoset) or 38.4×38.4 mm (rat), Matrix=256×256, Slice thickness=0.75 mm (marmoset) or 0.5 mm (rat), Slice orientation=horizontal, Number of slices=11, Number of averages=15), producing an in-plane resolution of 175 μm (marmoset) or 150 μm (rat). The sequence was repeated twice to span structures of interest in the brain. Baseline images were made before the infusion. The 40 mM MnCl₂ solution described previously was then infused into the tail-vein at 1.25 ml/h and images were made every 30 min until T₁-weighted enhancement was clearly seen in the periventricular tissue. For the marmoset, a total dose of 89 mg/kg MnCl₂ 4H₂O was injected over 180 min and six images were acquired. In the rat, a total dose of 71 mg/kg was injected over 120 min and 5 images were acquired. In light of the high manganese dose infused, animals were euthanized after imaging under 5% isoflurane with a lethal injection of sodium pentobarbital.

4.7. Image post-processing

All 3D images were registered into a common space using an affine registration and analyzed in Amira (Mercury Computer Systems, Houston, TX, USA). Regions-of-interest (ROIs) were drawn in structures identified by an atlas (Paxinos and Watson, 1998; Stephan et al., 1980) that could be clearly delineated in the T₁-weighted images and the lower-resolution T₁ maps from which mean signal intensities and T₁s were measured respectively. It was determined from the T₁ maps that there were no statistically significant changes in T₁ in either species in the muscle surrounding the skull following the manganese injections (*p*=1.00 in both cases). Thus, the mean T₁ signal intensity in muscle surrounding the skull in each animal was used to normalize the mean signal intensities from ROIs in other brain regions in the T₁-weighted images.

4.8. Interpretation of T₁-weighted images

The signal, *S*, in a brain region in a heavily T₁-weighted image is related to T₁ by the equation:

$$S = \kappa\rho(1 - e^{-TR/T_1}) \quad (1)$$

where κ is a catch-all gain constant, ρ is the tissue proton density, and TR is the repetition time of the pulse sequence. It can be assumed that κ is the same between the marmoset and rat images because the same MRI scanner, radiofrequency coil, pulse sequence, and image processing routines were used in the study. TR is the same because same pulse sequence was used. Finally, it is assumed that the tissue proton density is roughly the same between the same tissue types in the marmoset and rat. Thus, changes in the signal in T_1 -weighted images following manganese injections equivalently reflect T_1 changes in the two species.

The next question is how these T_1 changes relate to changes in tissue manganese concentration. Here, it is easier to work with the longitudinal relaxation rate, R_1 , which is inversely related to T_1 by the equation $R_1 = 1/T_1$. R_1 in a region is related to the tissue manganese concentration ($[Mn]$) by the equation:

$$R_1 = \chi_1([Mn]) + R_1(0) \quad (2)$$

where χ_1 is the longitudinal relaxivity and $R_1(0)$ is the longitudinal relaxation rate in tissue if there was no manganese. Neither MRI nor mass spectrometry can differentiate the oxidation states of manganese, so only the total manganese concentration in the tissue can be assessed. If χ_1 is the same between the species, then changes in R_1 (and hence, T_1) following manganese injections equivalently reflect changes in manganese concentration in the two species. By extension, signal changes in the T_1 -weighted images following manganese injections equivalently reflect changes in manganese concentration in the two species.

R_1 in various regions of brain of the two species was calculated from the T_1 maps made before and after manganese injections. χ_1 was calculated from a plot of R_1 against tissue manganese content measured in these same regions by mass spectrometry. Only gross brain regions were analyzed (the cortex, the striatum, the thalamus, and the hippocampus) because of the limited quality of the EPI-based T_1 maps. These regions were also readily identified and dissected from the excised brains and provided enough tissue for measurements of manganese content by mass spectrometry.

4.9. Statistics

Significant differences across the data were tested using a non-parametric analysis of variance (Kruskal-Wallis) performed in Systat 12 (Systat Software, San Jose, CA, USA) followed by a Bonferroni multiple-comparison test. Significant differences in slopes from linear regressions were tested with a Student's *t*-test using custom-written formulas in Excel (Microsoft Corporation, Redmond, WA, USA).

Acknowledgments

The authors would like to acknowledge the technical assistance of Julie Mackel, Sachy Sato, and Lisa Zhang and the veterinary care and advice of Dr. James O'Malley and Dr. Crystal Thomas. This research was supported by the Intramural Research Program of the NIH, NINDS (Alan P. Koretsky, Scientific Director). Nicholas Bock is the recipient of a Natural Sciences and Engineering Research Council of Canada post-doctoral fellowship.

REFERENCES

- Antonini, J.M., Santamaria, A.B., Jenkins, N.T., Albini, E., Lucchini, R., 2006. Fate of manganese associated with the inhalation of welding fumes: potential neurological effects. *Neurotoxicology* 27, 304–310.
- Aoki, I., Wu, Y.J., Silva, A.C., Lynch, R.M., Koretsky, A.P., 2004. In vivo detection of neuroarchitecture in the rodent brain using manganese-enhanced MRI. *Neuroimage* 22, 1046–1059.
- Aschner, M., Guilarte, T.R., Schneider, J.S., Zheng, W., 2007. Manganese: recent advances in understanding its transport and neurotoxicity. *Toxicol. Appl. Pharmacol.* 221, 131–147.
- Aschner, M., Erikson, K.M., Dorman, D.C., 2005. Manganese dosimetry: species differences and implications for neurotoxicity. *Crit. Rev. Toxicol.* 35, 1–32.
- Bock, N.A., Paiva, F.F., Silva, A.C., in press. Fractionated manganese-enhanced magnetic resonance imaging. *NMR Biomed.*
- Bowler, R.M., Gysens, S., Diamond, E., Nakagawa, S., Drezgic, M., Roels, H.A., 2006. Manganese exposure: neuropsychological and neurological symptoms and effects in welders. *Neurotoxicology* 27, 315–326.
- Cersosimo, M.G., Koller, W.C., 2006. The diagnosis of manganese-induced Parkinsonism. *Neurotoxicology* 27, 340–346.
- Chuang, K.H., Koretsky, A., 2006. Improved neuronal tract tracing using manganese enhanced magnetic resonance imaging with fast T(1) mapping. *Magn. Reson. Med.* 55, 604–611.
- Crossgrove, J., Zheng, W., 2004. Manganese toxicity upon over-exposure. *NMR Biomed.* 17, 544–553.
- Crossgrove, J.S., Allen, D.D., Bukaveckas, B.L., Rhineheimer, S.S., Yokel, R.A., 2003. Manganese distribution across the blood-brain barrier. I. Evidence for carrier-mediated influx of manganese citrate as well as manganese and manganese transferrin. *Neurotoxicology* 24, 3–13.
- Dobson, A.W., Erikson, K.M., Aschner, M., 2004. Manganese neurotoxicity. *Ann. N. Y. Acad. Sci.* 1012, 115–128.
- Dorman, D.C., Struve, M.F., Marshall, M.W., Parkinson, C.U., James, R.A., Wong, B.A., 2006a. Tissue manganese concentrations in young male rhesus monkeys following subchronic manganese sulfate inhalation. *Toxicol. Sci.* 92, 201–210.
- Dorman, D.C., Struve, M.F., Wong, B.A., Dye, J.A., Robertson, I.D., 2006b. Correlation of brain magnetic resonance imaging changes with pallidal manganese concentrations in rhesus monkeys following subchronic manganese inhalation. *Toxicol. Sci.* 92, 219–227.
- Erikson, K.M., Thompson, K., Aschner, J., Aschner, M., 2007. Manganese neurotoxicity: a focus on the neonate. *Pharmacol. Ther.* 113, 369–377.
- Guilarte, T.R., McGlothlan, J.L., Degaonkar, M., Chen, M.K., Barker, P.B., Syversen, T., Schneider, J.S., 2006. Evidence for cortical dysfunction and widespread manganese accumulation in the nonhuman primate brain following chronic manganese exposure: a 1H-MRS and MRI study. *Toxicol. Sci.* 94, 351–358.
- Gwiazda, R., Lucchini, R., Smith, D., 2007. Adequacy and consistency of animal studies to evaluate the neurotoxicity of chronic low-level manganese exposure in humans. *J. Toxicol. Environ. Health A* 70, 594–605.
- Henriksson, J., Tallkvist, J., Tjalve, H., 1999. Transport of manganese via the olfactory pathway in rats: dosage dependency of the uptake and subcellular distribution of the metal in the olfactory epithelium and the brain. *Toxicol. Appl. Pharmacol.* 156, 119–128.
- Jiang, Y., Zheng, W., Long, L., Zhao, W., Li, X., Mo, X., Lu, J., Fu, X., Li, W., Liu, S., Long, Q., Huang, J., Pira, E., 2007. Brain magnetic resonance imaging and manganese concentrations in red blood cells of smelting workers: search for biomarkers of manganese exposure. *Neurotoxicology* 28, 126–135.

- Kang, Y.S., Gore, J.C., 1984. Studies of tissue NMR relaxation enhancement by manganese. Dose and time dependences. *Invest. Radiol.* 19, 399–407.
- Klaassen, C.D., 1974. Biliary excretion of manganese in rats, rabbits, and dogs. *Toxicol. Appl. Pharmacol.* 29, 458–468.
- Klos, K.J., Chandler, M., Kumar, N., Ahlskog, J.E., Josephs, K.A., 2006. Neuropsychological profiles of manganese neurotoxicity. *Eur. J. Neurol.* 13, 1139–1141.
- Krieger, D., Krieger, S., Jansen, O., Gass, P., Theilmann, L., Lichtnecker, H., 1995. Manganese and chronic hepatic encephalopathy. *Lancet* 346, 270–274.
- Lee, J.H., Silva, A.C., Merkle, H., Koretsky, A.P., 2005. Manganese-enhanced magnetic resonance imaging of mouse brain after systemic administration of MnCl₂: dose-dependent and temporal evolution of T₁ contrast. *Magn. Reson. Med.* 53, 640–648.
- Lin, Y.J., Koretsky, A.P., 1997. Manganese ion enhances T₁-weighted MRI during brain activation: an approach to direct imaging of brain function. *Magn. Reson. Med.* 38, 378–388.
- Murayama, Y., Weber, B., Saleem, K.S., Augath, M., Logothetis, N.K., 2006. Tracing neural circuits in vivo with Mn-enhanced MRI. *Magn. Reson. Imaging* 24, 349–358.
- Murphy, V.A., Wadhvani, K.C., Smith, Q.R., Rapoport, S.I., 1991. Saturable transport of manganese(II) across the rat blood–brain barrier. *J. Neurochem.* 57, 948–954.
- Narita, K., Kawasaki, F., Kita, H., 1990. Mn and Mg influxes through Ca channels of motor nerve terminals are prevented by verapamil in frogs. *Brain Res.* 510, 289–295.
- Natt, O., Watanabe, T., Boretius, S., Radulovic, J., Frahm, J., Michaelis, T., 2002. High-resolution 3D MRI of mouse brain reveals small cerebral structures in vivo. *J. Neurosci. Methods* 120, 203–209.
- Olanow, C.W., Good, P.F., Shinotoh, H., Hewitt, K.A., Vingerhoets, F., Snow, B.J., Beal, M.F., Calne, D.B., Perl, D.P., 1996. Manganese intoxication in the rhesus monkey: a clinical, imaging, pathologic, and biochemical study. *Neurology* 46, 492–498.
- Pal, P.K., Samii, A., Calne, D.B., 1999. Manganese neurotoxicity: a review of clinical features, imaging and pathology. *Neurotoxicology* 20, 227–238.
- Park, N.H., Park, J.K., Choi, Y., Yoo, C.I., Lee, C.R., Lee, H., Kim, H.K., Kim, S.R., Jeong, T.H., Park, J., Yoon, C.S., Kim, Y., 2003. Whole blood manganese correlates with high signal intensities on T₁-weighted MRI in patients with liver cirrhosis. *Neurotoxicology* 24, 909–915.
- Pautler, R.G., Koretsky, A.P., 2002. Tracing odor-induced activation in the olfactory bulbs of mice using manganese-enhanced magnetic resonance imaging. *Neuroimage* 16, 441–448.
- Pautler, R.G., Mongeau, R., Jacobs, R.E., 2003. In vivo trans-synaptic tract tracing from the murine striatum and amygdala utilizing manganese enhanced MRI (MEMRI). *Magn. Reson. Med.* 50, 33–39.
- Paxinos, G., Watson, C., 1998. *The Rat Brain in Stereotaxic Coordinates*. Academic Press, New York.
- Rabin, O., Hegedus, L., Bourre, J.M., Smith, Q.R., 1993. Rapid brain uptake of manganese(II) across the blood–brain barrier. *J. Neurochem.* 61, 509–517.
- Saleem, K.S., Pauls, J.M., Augath, M., Trinath, T., Prause, B.A., Hashikawa, T., Logothetis, N.K., 2002. Magnetic resonance imaging of neuronal connections in the macaque monkey. *Neuron* 34, 685–700.
- Shinotoh, H., Snow, B.J., Hewitt, K.A., Pate, B.D., Doudet, D., Nugent, R., Perl, D.P., Olanow, W., Calne, D.B., 1995. MRI and PET studies of manganese-intoxicated monkeys. *Neurology* 45, 1199–1204.
- Sloot, W.N., Gramsbergen, J.B., 1994. Axonal transport of manganese and its relevance to selective neurotoxicity in the rat basal ganglia. *Brain Res.* 657, 124–132.
- Stephan, H., Baron, G., Schwerdtfeger, W.K., 1980. *The Brain of the Common Marmoset (Callithrix jacchus)*. Springer-Verlag, New York.
- Takeda, A., 2003. Manganese action in brain function. *Brain Res. Rev.* 41, 79–87.
- Takeda, A., Sawashita, J., Okada, S., 1995. Biological half-lives of zinc and manganese in rat brain. *Brain Res.* 695, 53–58.
- Tapin, D., Kennedy, G., Lambert, J., Zayed, J., 2006. Bioaccumulation and locomotor effects of manganese sulfate in Sprague–Dawley rats following subchronic (90 days) inhalation exposure. *Toxicol. Appl. Pharmacol.* 211, 166–174.
- Thompson, K., Molina, R.M., Donaghey, T., Schwob, J.E., Brain, J.D., Wessling-Resnick, M., 2007. Olfactory uptake of manganese requires DMT1 and is enhanced by anemia. *FASEB J.* 21, 223–230.
- Tjalve, H., Henriksson, J., Tallkvist, J., Larsson, B.S., Lindquist, N.G., 1996. Uptake of manganese and cadmium from the nasal mucosa into the central nervous system via olfactory pathways in rats. *Pharmacol. Toxicol.* 79, 347–356.
- Tjalve, H., Mejare, C., Borg-Neczak, K., 1995. Uptake and transport of manganese in primary and secondary olfactory neurones in pike. *Pharmacol. Toxicol.* 77, 23–31.
- Uchino, A., Noguchi, T., Nomiyama, K., Takase, Y., Nakazono, T., Nojiri, J., Kudo, S., 2007. Manganese accumulation in the brain: MR imaging. *Neuroradiology* 49 (9), 715–720.
- Wang, J., Qiu, M., Constable, R.T., 2005. In vivo method for correcting transmit/receive nonuniformities with phased array coils. *Magn. Reson. Med.* 53, 666–674.
- Wedler, F.C., Denman, R.B., 1984. Glutamine synthetase: the major Mn(II) enzyme in mammalian brain. *Curr. Top. Cell. Regul.* 24, 153–169.
- Zhang, S., Zhou, Z., Fu, J., 2003. Effect of manganese chloride exposure on liver and brain mitochondria function in rats. *Environ. Res.* 93, 149–157.